Proceedings of the PHOTON-2017 Conference, Geneva, Switzerland, 22 – 26 May 2017, edited by David d'Enterria, Albert de Roeck and Michelangelo Mangano, CERN Proceedings, Vol. 1/2018, CERN-Proceedings-2018-001 (CERN, Geneva, 2018)

Photon interactions in ultra-peripheral heavy-ion collisions in the ATLAS detector at the LHC

Samuel Webb on behalf of the ATLAS Collaboration
Johannes Gutenberg University Mainz, Mainz, Germany

Abstract

Two analyses involving photon interactions in ultra-peripheral lead-lead collisions in the ATLAS detector at the LHC are described, namely the study of dijet production in photo-nuclear ultra-peripheral collisions and a measurement of light-by-light scattering. The first, is an important way to probe and constrain nuclear parton distribution functions, which are known to exhibit suppression at low Bjorken-x with respect to proton PDFs, as well as enhancement at higher Bjorken-x. Light-by-light scattering is forbidden in classical electrodynamics as it violates the super-position principle and is a fundamental prediction of quantum mechanics. The first direct evidence for this interaction with two quasi-real initial state photons is presented.

Keywords
CERN report; PHOTON2017; photon-photon collisions; photon-lead collisions; light-by-light scattering; heavy-ion collisions; LHC; ATLAS

1 Introduction

Ultra-peripheral collisions (UPC) of heavy ions occur when the impact parameter is greater than twice the nuclear radius. In these events the strong interaction plays a limited role [1] and as such they provide an ideal environment for photon interaction studies. Additionally the high nuclear charge compared to proton-proton collisions gives an enhanced photon flux (by a factor of the nuclear charge, Z, squared), which compensates for the smaller integrated luminosity typical for such datasets.

A distinctive signature of such UPC events (which is employed in both analyses described) is that the ion emitting an initial state photon does not generally break-up, leaving a rapidity gap in the detector in the flight direction of the ion. Two ATLAS forward sub-detectors are particularly suited to identifying this characteristic signature, the Zero Degree Calorimeters (ZDC) and Minimum Bias Trigger Scintillators (MBTS). The ZDC are located ± 140m either side of the nominal interaction point [2], covering an absolute pseudorapidity range $|\eta| > 8.3$. Figure 1 shows an event display of an event which was obtained using a trigger that required one or more neutrons in the ZDC on one side and none on the other side [3]. The rapidity gap can be seen in the left half of the detector and note that the ZDC itself is not pictured. This trigger was used in the dijet production measurements described in Section 2. The octagonal sub-detectors shaded yellow are the MBTS. These are positioned between the Inner Detector and end-cap calorimeters with a coverage in absolute pseudorapidity between 2.07 and 3.86. The light-by-light scattering analysis (described in Section 3) employs a trigger which rejects events if more than one hit was found in the inner ring of the MBTS.

2 Photo-nuclear dijet production in ultra-peripheral Pb+Pb collisions

This section summarises the analysis described in Ref. [4], namely the study of several event-level observables in events with two or more jets produced via photo-nuclear interactions in UPC lead-lead (Pb+Pb) collisions in the ATLAS detector. The data was taken in 2015 at a centre of mass energy per nucleon pair of 5.02 TeV.

https://doi.org/10.23727/CERN-Proceedings-2018-001.137

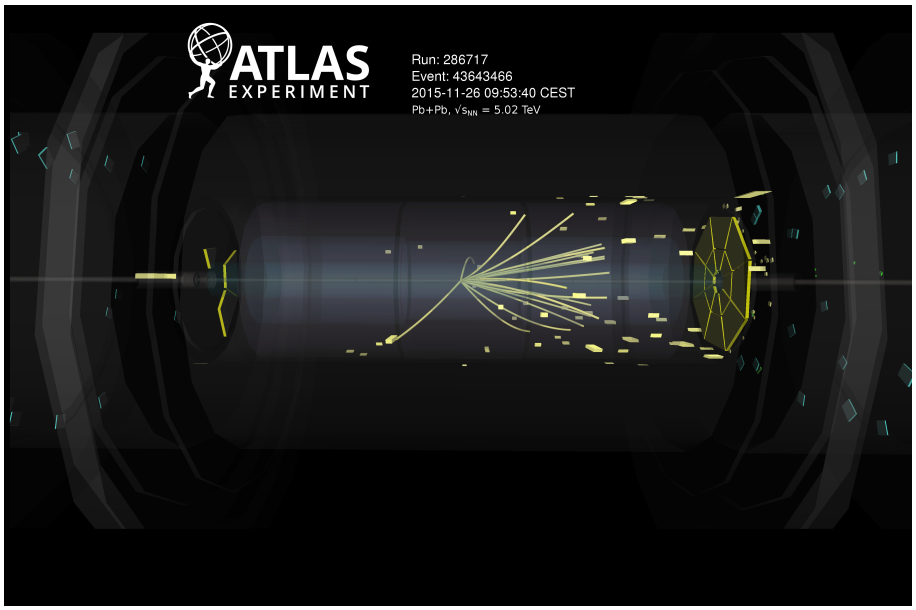

Fig. 1: Display of an event with large rapidity gap taken with the ZDC_XOR trigger, firing on more than one spectator neutrons on one side and no neutrons on the other side. The rapidity gap is on the side with no neutrons in the ZDC. The MBTS sub-detectors are also shown, shaded in yellow [3].

2.1 Motivation

The motivation for such measurements is to probe the nuclear parton distribution functions (PDFs), which are known to differ from proton PDFs [5]. At parton momentum fraction values below $x \approx 0.03$ the nuclear cross-section is suppressed (known as 'shadowing'), whilst at higher values of x between about 0.03 and 0.3 an enhancement (or 'anti-shadowing') is observed. Knowledge of the nuclear PDFs at low-x is however limited by the lack of experimental data [4] - an issue that this analysis addresses.

In addition to the factor of Z^2 enhancement with respect to the same process in proton-proton collisions, the cross-section is further increased by a Lorentz boost factor giving a total enhancement of 1.5×10^6 extending to initial state photon energies of 50 GeV [4].

2.2 Observables and measurements

The process of interest in this measurement can be separated into two scenarios. The first is known as direct photo-production and is shown in the left panel of Figure 2 [4]. In this case the nucleus emitting the initial state photon remains intact forming a clear rapidity gap in the flight direction of the nucleon. The other nucleus breaks up and no rapidity gap is seen. The other scenario is known as resolved photo-production, shown in the right panel of Figure 2. In this case the initial state photon serves as a source of partons which go on to participate in the hard interaction. The rapidity gap is then partially filled.

Events of interest are selected for study using a set of three triggers. Each of these require zero neutrons to be detected in one of the ZDCs (defined to be the photon-going direction), and one or more neutrons in the ZDC on the opposite side, as well as the sum of transverse energy measured in the calorimeters to be between 5 and 200 GeV. Two of the triggers have additional requirements on the transverse momentum, p_T, and pseudorapidity of jets. The total luminosity sampled by these triggers is 380 μb^{-1}.

Background events are rejected by employing rapidity gap requirements on each side. Firstly clusters and charged particle tracks are ordered in η and intervals between adjacent tracks or clusters with separation $\Delta\eta > 0.5$ are recorded. The rapidity gap sum, $\Sigma\Delta\eta$, is required to be greater than 2 on

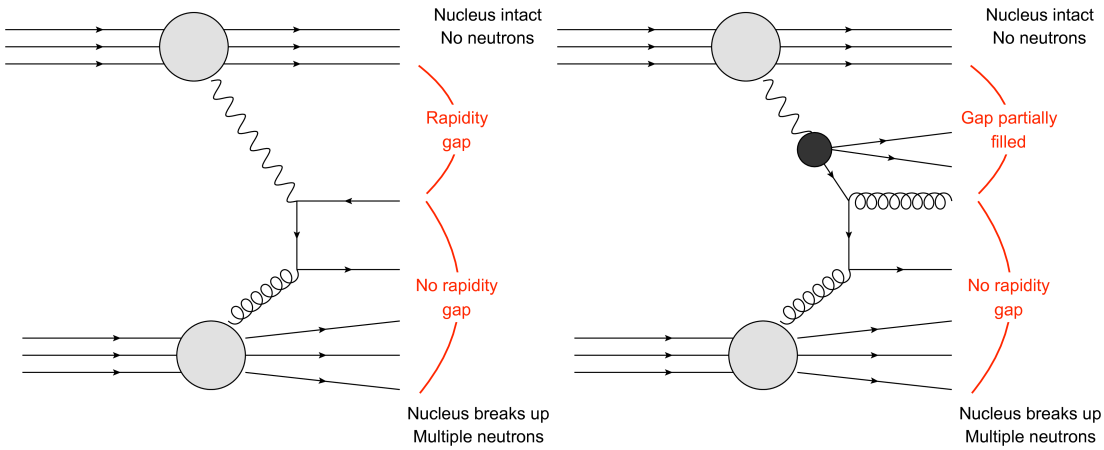

Fig. 2: Diagrams representing different types of leading-order contributions to dijet production in high-energy photo-nuclear collisions. The left diagram represents the direct contribution in which the photon itself participates in the hard scattering. The right diagram represents the 'resolved' contribution in which virtual excitations of the photon, into a state involving at least a $q\bar{q}$ pair and possibly multiple gluons, participates in the hard scattering in the target nucleus [4].

the photon-going side, and less than 3 on the opposite side (in order to reduce contamination from $\gamma+\gamma$ collisions and non-photo-nuclear UPC processes) [4]. Events are then required to have at least two jets with $p_{\mathrm{T}} > 20$ GeV and $|\eta| < 4.4$. Jets are reconstructed using the anti-k_t algorithm with $R = 0.4$ [6] and with a heavy ion subtraction technique described in Ref. [7].

Three event-level variables are formed from the selected jets in an event and are defined in Equation 1, where i runs over the measured jets in an event, E is the jet energy, $\vec{p}$ is the jet momentum, and p_z is the longitudinal component of that momentum.

$$H_{\mathrm{T}} \equiv \sum_i p_{Ti}, \quad m_{\mathrm{jets}} \equiv \left[\left(\sum_i E_i\right)^2 - \left|\sum_i \vec{p_i}\right|^2\right]^{1/2}, \quad y_{\mathrm{jets}} \equiv \frac{1}{2}\ln\left(\frac{\sum_i E_i + \sum_i p_{z,i}}{\sum_i E_i - \sum_i p_{z,i}}\right) \tag{1}$$

Two derived quantities can then be formed using m_{jets} (the jet system mass) and y_{jets} (the jet system rapidity). These are defined in Equation 2, where x_{A} corresponds to the ratio of the energy of the struck parton in the nucleus to the (per nucleon) beam energy and z_γ is the equivalent quantity for the photon (multiplied by the fraction of the photon's energy carried by the resolved parton, in the resolved photo-production scenario).

$$x_{\mathrm{A}} \equiv \frac{m_{\mathrm{jets}}}{\sqrt{s}} e^{-y_{\mathrm{jets}}}, \quad z_\gamma \equiv \frac{m_{\mathrm{jets}}}{\sqrt{s}} e^{+y_{\mathrm{jets}}} \tag{2}$$

A triple-differential cross section is defined in Equation 3, where ΔN is the number of events measured in a particular bin of width ΔH_{T}, Δx_{A} and Δz_γ in the variables H_{T}, x_{A} and z_γ respectively. The integrated luminosity is labelled $\mathcal{L}$ and ϵ_{sel} and ϵ_{trig} are the selection and trigger efficiencies. Note that no correction is made for the detector response, which is indicated by the tilde on the cross-section σ. This cross-section is presented in various 2D and 1D slices.

$$\frac{d^3\tilde{\sigma}}{dH_{\mathrm{T}} dx_{\mathrm{A}} dz_\gamma} = \frac{1}{\mathcal{L}} \frac{\Delta N}{\Delta H_{\mathrm{T}} \Delta x_{\mathrm{A}} \Delta z_\gamma} \frac{1}{\epsilon_{\mathrm{trig}} \epsilon_{\mathrm{sel}}} \tag{3}$$

2.3 Results and comparison to theory

PYTHIA version 6.41 [8] is used to simulate the photo-nuclear events using the equivalent photon flux from a muon beam as the source of photons. This provides the correct mixture of direct and resolved processes, however the photon energy spectrum in this Pythia version is not appropriate for nuclear collisions. The predicted spectrum is therefore reweighted to that from STARLIGHT [9], a MC model and event generator that has been used to simulate two-photon and photon-pomeron scattering in heavy ion collisions. STARLIGHT has been tested using data from both RHIC and LHC including the ATLAS measurement of $\gamma + \gamma \to \mu^+\mu^-$ in 5.02 TeV Pb+Pb collisions [10]. STARLIGHT was found in that particular measurement to reproduce the shape and normalisation of the di-muon spectrum well, indicating the photon flux is under control.

The necessity of reweighting the energy spectrum is demonstrated in Figure 3. Here the distributions of z_γ and the rapidity gap on the photon-going side, $\Sigma_\gamma \Delta\eta$, are shown for data (black points), the nominal PYTHIA model (blue points), and for PYTHIA reweighted to STARLIGHT (red points). The reweighted model is in much better agreement with data than the nominal model.

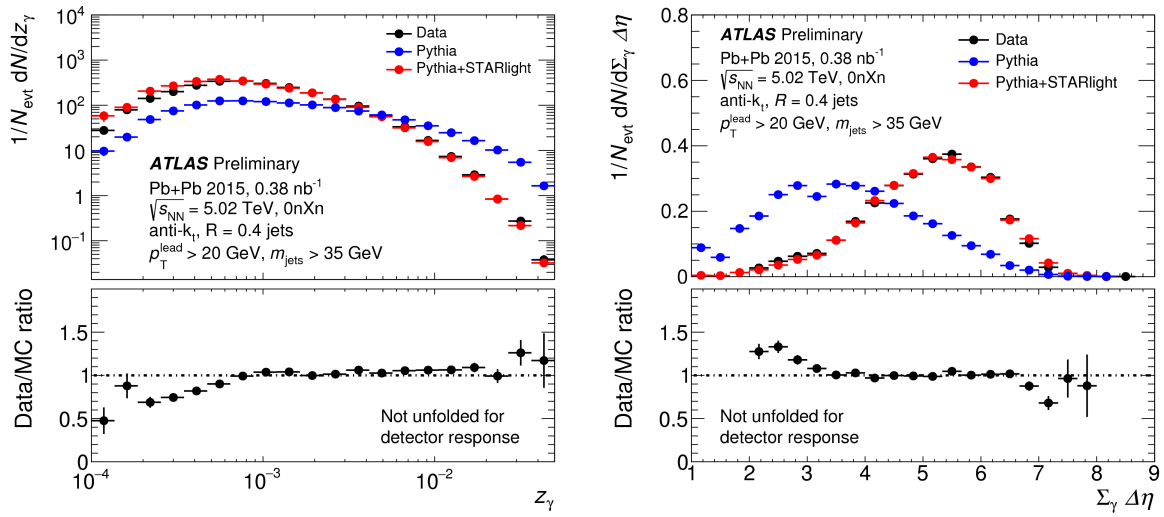

Fig. 3: Comparison of data (black points) and PYTHIA MC before (blue points) and after (red points) reweighting to STARLIGHT. The left figure shows the z_γ distribution, and the right figure shows the $\Sigma_\gamma \Delta\eta$ distribution. The bottom panels shows the ratio of data to the reweighted model. The error bars represent the statistical uncertainties only. [4].

Two examples of the final cross-section distributions are shown in Figure 4. The left plot shows the double differential cross-section $d^2\tilde{\sigma}/dH_{\mathrm{T}}dz_\gamma$ as a function of z_γ for different intervals of H_{T}. The right plot shows $d^2\tilde{\sigma}/dz_\gamma dx_{\mathrm{A}}$ as a function of x_{A} for different intervals of z_γ. Data is shown in comparison to PYTHIA MC reweighted to STARLIGHT. The statistical uncertainty on the data is shown as error bars and the systematic uncertainty is shown as shaded bands. Not shown is the uncertainty on the cross-section normalisation (6.2%) which comes mostly from the integrated luminosity uncertainty (6.1%). The largest systematic uncertainties are due to the event selection efficiency, specifically the requirements on $\Sigma\Delta\eta$ which are between 10-25% depending on x_{A}, and the jet energy scale and resolution, which can be up to 40% depending on the H_{T}, x_{A} and z_γ. Generally the model is in good agreement with data, except at the lowest values of z_γ and x_{A}, where the cross-sections are particularly sensitive to the kinematic selections.

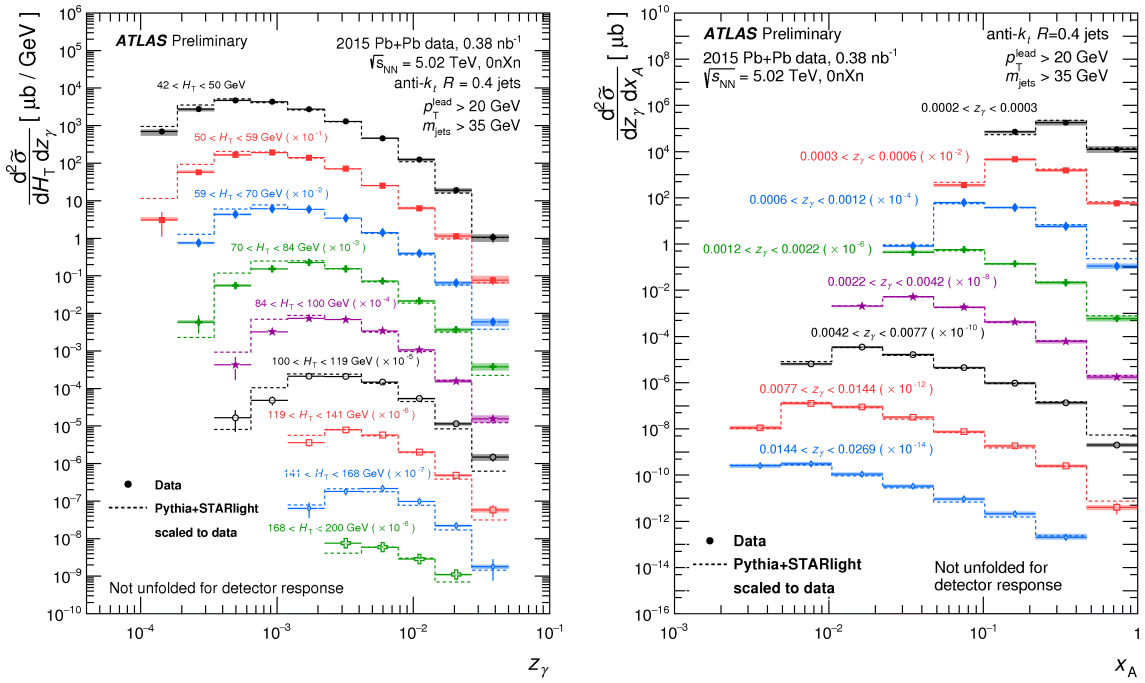

Fig. 4: The left plot shows the double differential cross-section $d^2\tilde{\sigma}/dH_{\mathrm{T}}dz_\gamma$ as a function of z_γ for different intervals of H_{T}. The right plot shows $d^2\tilde{\sigma}/dz_\gamma dx_{\mathrm{A}}$ as a function of x_{A} for different intervals of z_γ [4].

3 Evidence for light-by-light scattering in heavy-ion collisions with the ATLAS detector at the LHC

This section summarises the analysis described in Ref. [1], which provides evidence for the process $\gamma\gamma \to \gamma\gamma$ or 'light-by-light scattering' in UPC Pb+Pb collisions in the ATLAS detector. This analysis uses the same 2015 dataset as the dijet analysis.

3.1 Introduction

The light-by-light scattering process is a purely quantum mechanical effect forbidden in classical electrodynamics as it violates the superposition principle [1]. In QED the reaction proceeds at lowest order via box diagrams involving fermions, which is an $\mathcal{O}\left(\alpha_{\mathrm{EM}}^4\right)$ process. Feynman diagrams for light-by-light scattering as well as two related processes with higher photon virtuality (Delbrück scattering of a photon in the Coulomb field of a nucleus, and photon-splitting via interaction with external fields) are shown in Figure 5. Delbrück scattering and photon-splitting have previously both been directly observed but evidence for low virtuality (or 'quasi-real') light-by-light scattering exists only indirectly from measurements of the anomalous magnetic moments of the electron and muon.

The signature for such a process in ATLAS is two low-energy photons and no further activity in the central detector. Typically this measurement could not be performed with proton-proton collisions where the average number of interactions per bunch crossing (pileup) is higher. A further advantage of using the Pb+Pb dataset is that the cross-section is enhanced by the high nuclear charge (as for the dijet measurement) [11]. This more than compensates the fact that the integrated luminosity is much smaller than the proton-proton datasets.

The signal light-by-light Monte Carlo (MC) samples are generated using calculations from Ref. [12]. The calculations are convolved with the Pb+Pb equivalent photon approximation spectrum from STARLIGHT. The resulting predictions are cross-checked with those from Ref. [11] and found to be in good agreement.

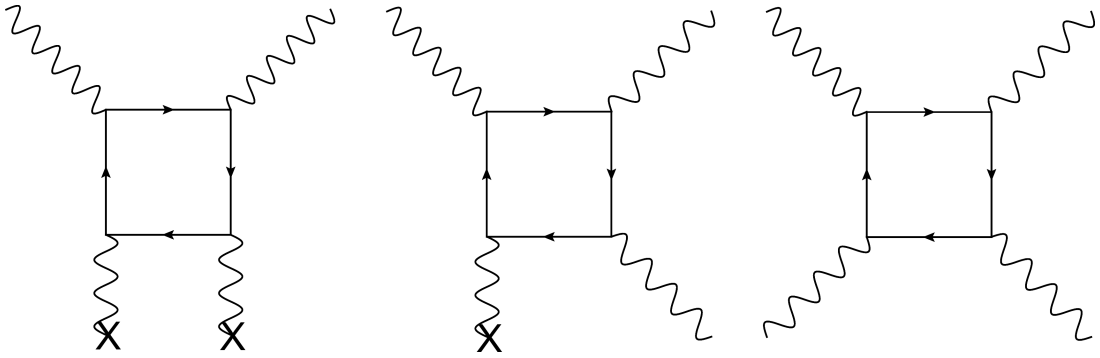

Fig. 5: Diagrams illustrating the QED light-by-light interaction processes: Delbrück scattering (left), photon splitting (middle) and elastic light-by-light scattering (right) [1].

The theoretical uncertainties on the model are mainly due to limited knowledge of the electromagnetic form factors and the initial photon fluxes (conservatively estimated to be 20%) and of higher order corrections (a few percent).

3.2 Photon identification and event selection

The final state photons in the process of interest typically have a transverse energy, E_{T}, between 3 and 20 GeV, which is lower than in most other ATLAS analyses. Therefore a dedicated photon identification technique is used and detailed studies of the photon reconstruction and identification efficiencies are performed.

Photons are reconstructed from electromagnetic clusters in the calorimeter and with tracking information from the Inner Detector in order to identify photon conversions. The reconstruction efficiency is measured using $\gamma\gamma \to e^+e^-$ events which have emitted a hard bremsstrahlung photon. The data and model are found to have similar efficiencies as a function of the photon E_{T} and an uncertainty of between 5% and 10% is applied to cover any residual differences.

Photons are identified using three shower shape variables (a sub-set of the variables used for standard ATLAS photon identification). The identification is optimised using a multi-variate technique in order to maintain a constant efficiency of 95% as a function of η. The identification efficiency is measured using $\gamma\gamma \to \ell^+\ell^-$ events with a final state radiation photon. The efficiencies of the data and of the model are found to agree within the statistical precision and an uncertainty of up to 10% is applied.

The trigger used to select candidate events requires the sum of transverse energy measured in the calorimeters to be between 5 and 200 GeV, there to be 1 hit or less in the MBTS inner ring, and 10 hits or less in the pixel detector. A total luminosity of $480\ \mu\mathrm{b}^{-1}$ is sampled by this trigger, which has a relative uncertainty of 6%. Events are then required to have two photons with an $E_{\mathrm{T}} > 3$ GeV and $|\eta| < 2.37$ excluding the calorimeter transition region $1.37 < |\eta| < 1.52$. The two-photon system is also required to have an invariant mass, $m_{\gamma\gamma}$ above 6 GeV and a transverse momentum less than 2 GeV to reduce backgrounds. Events are vetoed if a charged track is reconstructed in the pixel detector to reduce the background from $\gamma\gamma \to e^+e^-$ events and finally it is demanded that the photons are back to back, i.e. the acoplanarity $\mathrm{Aco} = 1 - \Delta\phi/\pi < 0.01$, to reduce the central exclusive production (CEP) $gg \to \gamma\gamma$ background. 13 data events pass all of the cut criteria. Figure 6 shows the distributions of diphoton invariant mass and absolute rapidity for data and the model. Good agreement is seen between the two.

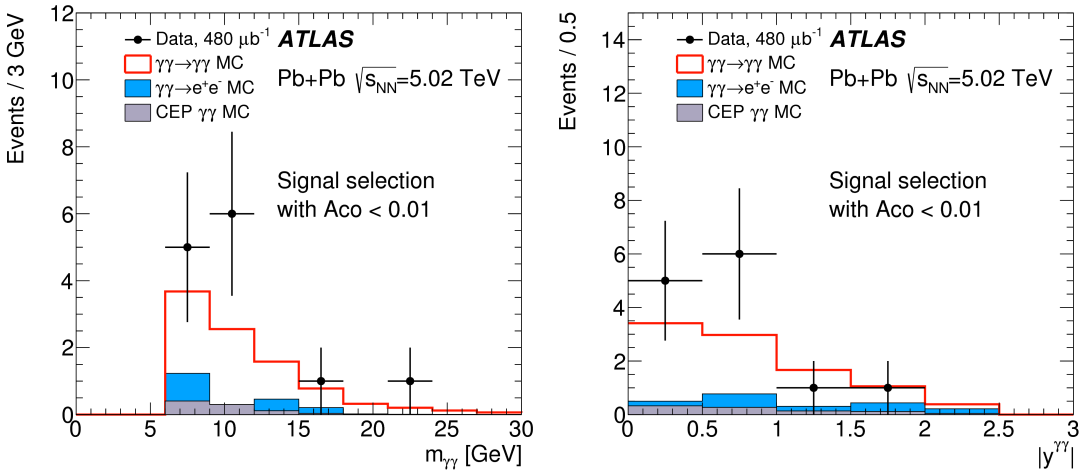

Fig. 6: Kinematic distributions for $\gamma\gamma \to \gamma\gamma$ event candidates: the diphoton invariant mass (left), the diphoton absolute rapidity (right). Data (points) are compared to MC expectations (histograms) [1].

3.3 Backgrounds

The dominant background comes from the process $\gamma\gamma \to e^+e^-$, due to its high rate as well as the fact that it has a peak at low acoplanarity like the signal. This is estimated with MC and then verified in control regions which require exactly one, or exactly two tracks to be identified. The process contributes 1.3 events in the signal region and is assigned an uncertainty of 25% based on the limited data statistics in the control regions. The other important background is CEP $gg \to \gamma\gamma$, which is again estimated with MC. This has a large theoretical uncertainty so a data-driven normalisation is performed in the acoplanarity distribution. The estimated contribution of this background in the signal region is 0.9 ± 0.5 events. Smaller and negligible backgrounds also considered are $\gamma\gamma \to q\bar{q} \to$ multiple π^0 mesons, exclusive neutral two-meson production and fake events, for example cosmic-ray muons.

3.4 Results

Figure 7 shows the final $\gamma\gamma$ acoplanarity distribution (without the Aco cut) [1]. In the region Aco < 0.01 13 data events are observed where 7.3 signal events and 2.6 background events were expected. This gives a significance of 4.4σ over the background-only hypothesis.

The data is then corrected for selection inefficiencies and the impact of the photon energy and angular resolution to obtain a fiducial cross section of 70 ± 24 (stat.) $\pm$ 17 (syst.) nb. The dominant contributions to the total systematic uncertainty come from the photon reconstruction and identification efficiency determination, as well as the photon energy resolution estimate.

4 Summary

Ultra-peripheral lead-lead collisions are an ideal environment to study photo-nucleon and photon-photon collisions due to the high photon flux and little additional activity originating from the ion emitting the photon. Two results using events from UPC lead-lead collisions have been presented: dijet production in photo-nuclear interactions, and evidence for light-by-light scattering.

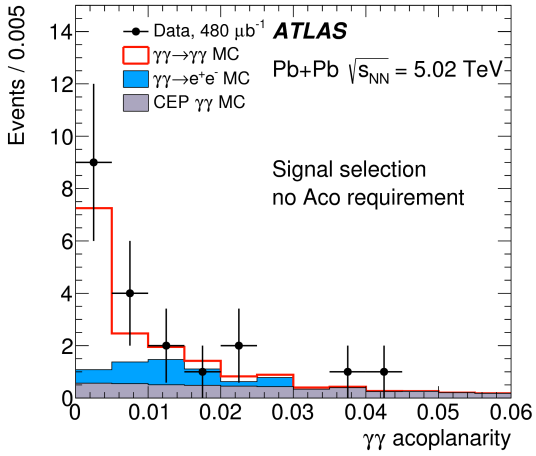

Fig. 7: The diphoton acoplanarity before applying Aco<0.01 requirement. Data (points) are compared to MC predictions (histograms). The statistical uncertainties on the data are shown as vertical bars. [1].

References

[1] The ATLAS Collaboration. Evidence for light-by-light scattering in heavy-ion collisions with the ATLAS detector at the LHC, 2017; *Nature Phys.*, 10.1038/nphys4208, arXiv:1702.01624 [hep-ex].

[2] The ATLAS Collaboration. The ATLAS Experiment at the CERN Large Hadron Collider. *JINST* 3 (2008) S08003.

[3] The ATLAS Collaboration. Performance plots for pp and Pb+Pb collisions at $\sqrt{s_{\rm NN}}$ = 5.02 TeV, https://atlas.web.cern.ch/Atlas/GROUPS/PHYSICS/PLOTS/HION-2015-001/

[4] The ATLAS Collaboration. Photo-nuclear dijet production in ultra-peripheral Pb+Pb collisions. ATLAS-CONF-2017-011, 2017. https://cds.cern.ch/record/2244822

[5] Hannu Paukkunen. Nuclear PDFs in the beginning of the LHC era. *Nucl. Phys.* A 926 (2014) 24, arXiv:1401.2345 [hep-ph].

[6] Matteo Cacciari, Gavin P. Salam, and Gregory Soyez. The Anti-k(t) jet clustering algorithm. *JHEP* 04 (2008) 063, arXiv:0802.1189 [hep-ph].

[7] The ATLAS Collaboration. Measurement of the jet radius and transverse momentum dependence of inclusive jet suppression in lead-lead collisions at $\sqrt{s_{NN}}$= 2.76 TeV with the ATLAS detector. *Phys. Lett.* B719 (2013) 220, arXiv:1208.1967 [hep-ex].

[8] Torbjorn Sjöstrand, Stephen Mrenna, and Peter Z. Skands. PYTHIA 6.4 Physics and Manual. *JHEP* 05 (2006) 026, arXiv:0603175 [hep-ph].

[9] Spencer R. Klein, Joakim Nystrand, Janet Seger, Yuri Gorbunov, and Joey Butterworth. STARlight: A Monte Carlo simulation program for ultra-peripheral collisions of relativistic ions. *Comput. Phys. Commun.* 212 (2017) 258, arXiv:1607.03838 [hep-ph].

[10] The ATLAS Collaboration. Measurement of high-mass dimuon pairs from ultra-peripheral lead-lead collisions at $\sqrt{s_{\rm NN}}$ = 5.02 TeV with the ATLAS detector at the LHC, ATLAS-CONF-2016-025, 2016, https://cds.cern.ch/record/2157689.

[11] David d'Enterria and Gustavo G. da Silveira. Observing light-by-light scattering at the Large Hadron Collider. *Phys. Rev. Lett.*, 111 (2013) 080405, [Erratum: *Phys. Rev. Lett.* 116 (2016) 129901], arXiv:1305.7142 [hep-ph].

[12] Mariola Klusek-Gawenda, Piotr Lebiedowicz and Antoni Szczurek, Light-by-light scattering in ultra-peripheral Pb-Pb collisions at energies available at the CERN Large Hadron Collider *Phys. Rev. C* 93 (2016) 044907, arXiv:1601.07001 [nucl-th].